# Large Scale Anomalous Patterns of Muscovite Mica Discovered by Atomic Force Microscopy

Feng Zhang,* Ping Zhang, Jiahua Hou, Xiaoling Yun, Wanrong Li, Qiqige Du, and Youjun Chen

School of Life Science, Inner Mongolia Agricultural University, 306 Zhaowuda Road, Hohhot 010018, China

ABSTRACT: Muscovite mica is a widely used substrate because of its flatness. The large scale anomalous patterns of muscovite have been discovered by atomic force microscopy (AFM). These patterns distribute around the defects of the muscovite surface. By using different imaging modes and analyzing functions of AFM, these extraordinary patterns are thoroughly characterized, and it was revealed that some selected regularly aligned patterns mimic 2-D orthorhombic crystal systems surrounding the regular structure. However, such patterned nanostructures have no effects on the template-assisted self-assembly (or epitaxial growth) of a disease-related peptide GAV-9.
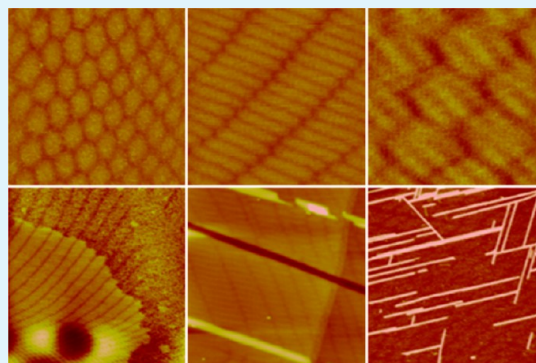
KEYWORDS: muscovite mica, atomic force microscopy, pattern, substrate, self-assembly

INTRODUCTION

Crystalline muscovite mica can be classified as one of the most favorite substrate materials for studying biological specimens,[1−7] epitaxial growth of metal nanostructures[8−11] and template-assisted self-assembling of biomolecules.[4,12−16] Not only can it be cleaved with great ease and down to thicknesses of a few hundred angstroms to produce very large, atomically flat, and chemically inert surfaces parallel to the [001] planes, but it is also available in high-grade natural and synthetic forms and shows reasonable thermal stability up to 700 °C.[17] More recently, the high affinity of the muscovite mica surface toward DNA, oligonucleotides, and lipids makes muscovite mica a possible template in the hypothesis of a surface mediated origin of life.[18,19]

Muscovite mica belongs to the family of clay minerals and the crystal structure of mica was first studied in 1927 with a chemical formula of $KAl_2(Si_3Al)O_{10}(OH)_2$.[20] The atomic structure of bulk mica[21] consists of sheets of negatively charged octahedral aluminosilicate layers in which the negative charge of the layers arises from a substitution of a quarter of the Si^{4+} ions by Al^{3+} ions. These layers are kept together by electrostatically bound interlayer cations, namely potassium ions (K^+), compensating the charge. Due to weak ionic bonding, mica is susceptible to cleavage along the [001] plane located in the potassium layer; therefore, a cleaved mica surface exhibits a hexagonal arrangement of Si (partly Al) and O atoms. However, this surface can be expected to be partly covered by potassium ions from the cationic layer.[22] It has been claimed that upon cleavage, the atomic structure of the aluminosilicate layers is undisturbed while the potassium layer is disrupted.[23]

To interpret and predict the adsorption and possible reaction of different materials on the mica surface, it is of greatest importance to understand the structure and morphology of cleaved mica surfaces down to the atomic scale. Normally, the freshly cleaved muscovite mica can be atomically flat up to the millimeter scale.[22,24] However, here we discovered the extraordinary patterns on some special regions of the freshly cleaved muscovite mica surface, which have been characterized by using different imaging modes and analyzing functions of atomic force microscopy (AFM). In principle, the synthetic growth of crystals[25] can be guided by the molecular recognition at interfaces with the micropatterned substrates which can be obtained by soft lithography[26−28] and ion beam sputtering.[29,30] Nevertheless, such anomalous nanostructures show nothing with the template-assisted self-assembly of a disease related peptide GAV-9 on the muscovite surface.

EXPERIMENTAL SECTION

Muscovite mica ($KAl_2(Si_3Al)O_{10}(OH)_2$, Sichuan Meifeng Co., China) was freshly cleaved by adhesive tape prior to each experiment. The peptide GAV-9 (NH_2-VGGAVVAGV-$CONH_2$) was custom-synthesized from China Peptides Co., Ltd. The sample had a purity of 98.3%, which was verified by high performance liquid chromatography (HPLC) and further characterized with mass spectrum. The lyophilized powder was stored at −20 °C. Before used, the peptide powder was dissolved in deionized water to a certain peptide concentration. Then the solutions were centrifuged at 10000 rpm for 10 min to get rid of any possible aggregates, and the supernatant was immediately used or distributed in aliquots to different PE tubes and kept in a freezer (−20 °C).

All AFM images were obtained with a commercial AFM instrument (Nanoscope IIId, Bruker) equipped with a J-scanner (125 × 125 μm). Both the contact mode and tapping mode in air were performed to
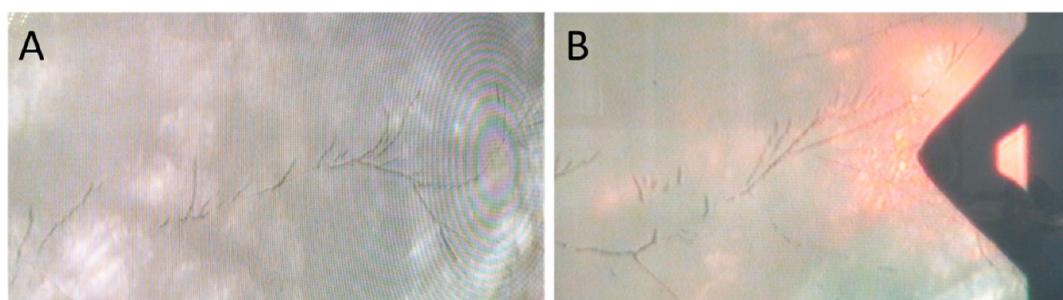
Figure 1. Wrinkled regions of muscovite mica surface under optical microscopy (∼200× magnification). The circles/rings in panel A are caused by light diffraction but not the real patterns of mica, and the red light in panel B was the laser point and the triangle is the AFM cantilever.
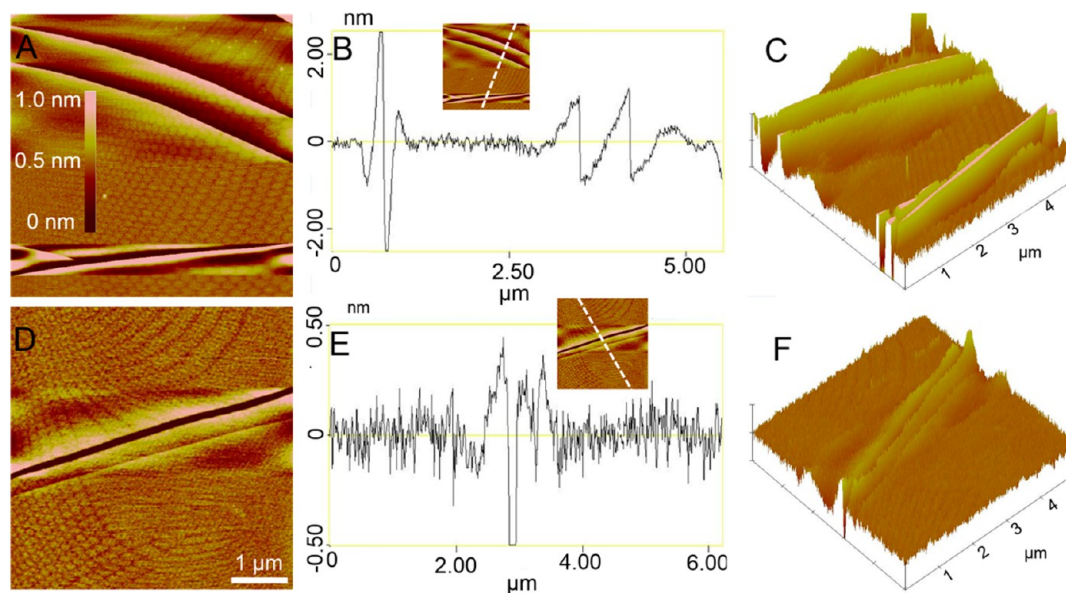

Figure 2. Large scale anomalous structures beside the wrinkled regions on the surface of muscovite mica. Deep grooves shown in height view (A), section analysis view (B), and 3-D view (C). Discrete radial patterns beside a groove in height view (D), section analysis view (E), and 3-D view (F). All AFM images were obtained by using tapping mode. The height bar and length bar applied to both height images. The white dotted lines in the insets indicate the section cutting lines.

observe the patterns. Commercial silicon cantilevers with normal spring constants of ∼48 N/m and a resonant frequency of ∼300 kHz (Tap300 AI-G, Budget Sensors) were used for the air tapping mode imaging. All images were captured with a scan rate at 1−2 Hz and 256 samples × 256 lines resolution. Silicon nitride cantilevers with a nominal spring constant of 0.35 N/m (SNL-10, Bruker) were used for air contact mode and tapping mode in liquid. After filling the as-prepared peptide solution in the liquid cell, AFM imaging was started immediately to study the dynamics of peptide assembly. AFM images were processed with the Flatten function to remove any tilts during imaging and analyzed with the Offline software (Digital Instrument, Version 5.12) that was supplied by the AFM manufacture.

■ RESULTS AND DISCUSSION

A mica surface that is freshly cleaved along the [001] plane located in the potassium layer usually can be used as a super flat substrate for AFM imaging. However, it is still possible to find some defects, which are defined as anything that could destroy the flatness of mica surface in this paper. The muscovite mica sheets provided by the commercial corporations have probabilities for some wrinkle-like defects on their surfaces, and a few of these wrinkles might not be visualized without the help of microscopy. As a substrate, these regions would normally be abandoned by scientists who might consider these regions to be a failure of a peeling procedure. However,

meticulous observation of these regions reveals interesting, amazing, and extraordinary patterns. As shown in Figure 1, the wrinkles on the muscovite surface can be observed under optical microscopy with a magnification of ∼200×. AFM is an eminent research tool used for the surface imaging and analyzing, here both the tapping and contact AFM modes were employed to further analyze the detailed surface structures at the nanometer scale.

Around the apparent defects such as the groove-like structures in Figure 2, there exhibits the strange patterns just on the freshly cleaved muscovite mica surface. From the section analysis of the grooves (Figure 2B), the depth is determined to be ∼1.0−3.5 nm. From Figure 2D, the patterns apparently show two radial circles that are separated by a groove in between. These patterns normally distribute around the defects of the muscovite mica surface, and the size of the patterned region can be over millimeter scale.

From Figure 3A, it is clear to see that the patterned region is separated by the step-edges of mica in a large scale (10×10 μm), and the patterns remain consistent on the two sides of the step-edges. And from the section analysis of the step-edge (Figure 3B), the peak-to-valley height of ∼0.5 nm equals to 1/2 step (1.002 nm) along the c-axis (muscovite mica is monoclinic crystal with the cell parameters as $a = 0.519\,06$ nm, $b = 0.9008$
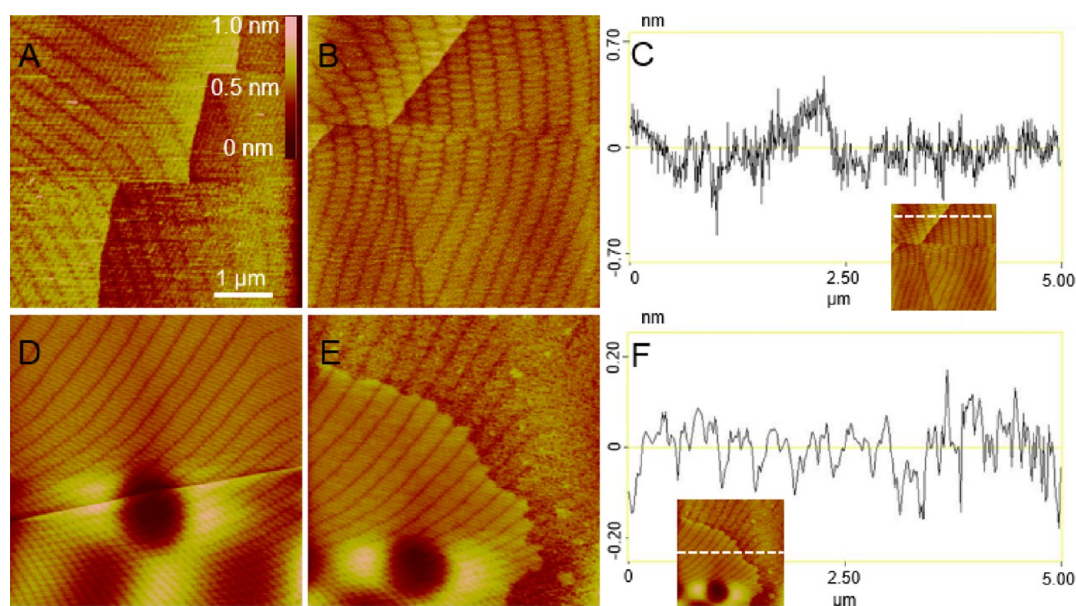
Figure 3. Anomalous patterns comparison between mica layers. Panels A, B, D, and E are the height view images obtained by using tapping mode AFM. Both the height and length bars applied to all these height images. Panel A shows the coexistence of two layers and panel B shows the disfigured patterns in a same layer. Panel E shows the surface topography of the same mica in panel D after peeling off its top layer. Panels C and F are the section analysis views for panels B and E, respectively. The white dotted lines in the insets indicate the section cutting lines.
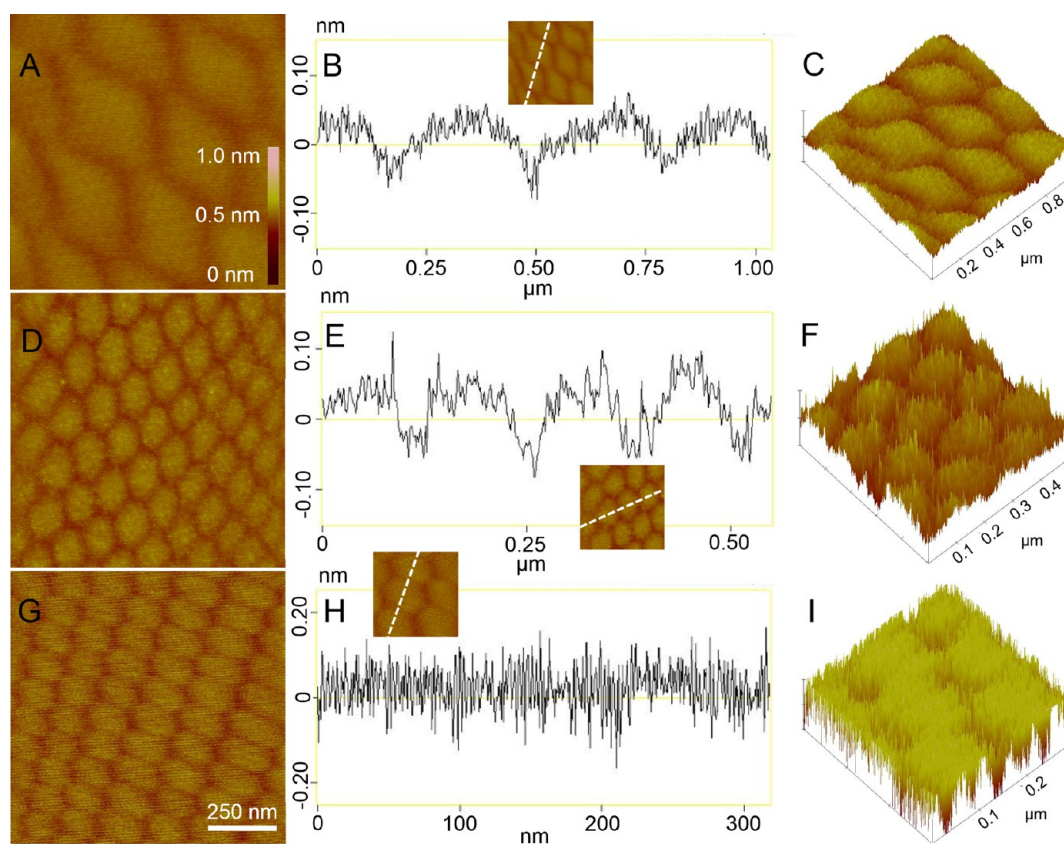

Figure 4. First group of regular patterns on the muscovite mica surface. Both panels A and D were obtained by tapping mode AFM, and panel G is a contact mode AFM image. Both the height and length bars apply to all these three height view images (A, D, and G). Panels B, E, and H are the section analysis views for panels A, D, and G, respectively. The white dotted lines in the insets indicate the section cutting lines. Panels C, F, and I are the 3-D views of panels A, D, and G, respectively.

nm, c = 2.0047 nm, β = 95.757°, space group $C2/c$).[24] The patterns from the upper layer develop their shapes continuously without any orientation mismatches when crossing the half

step-edges. In addition, it is also clear to see there is a bended mismatched "line" in the pattern (Figure 3B), which leads to the rod-like units becoming narrow and disfigured, respectively.
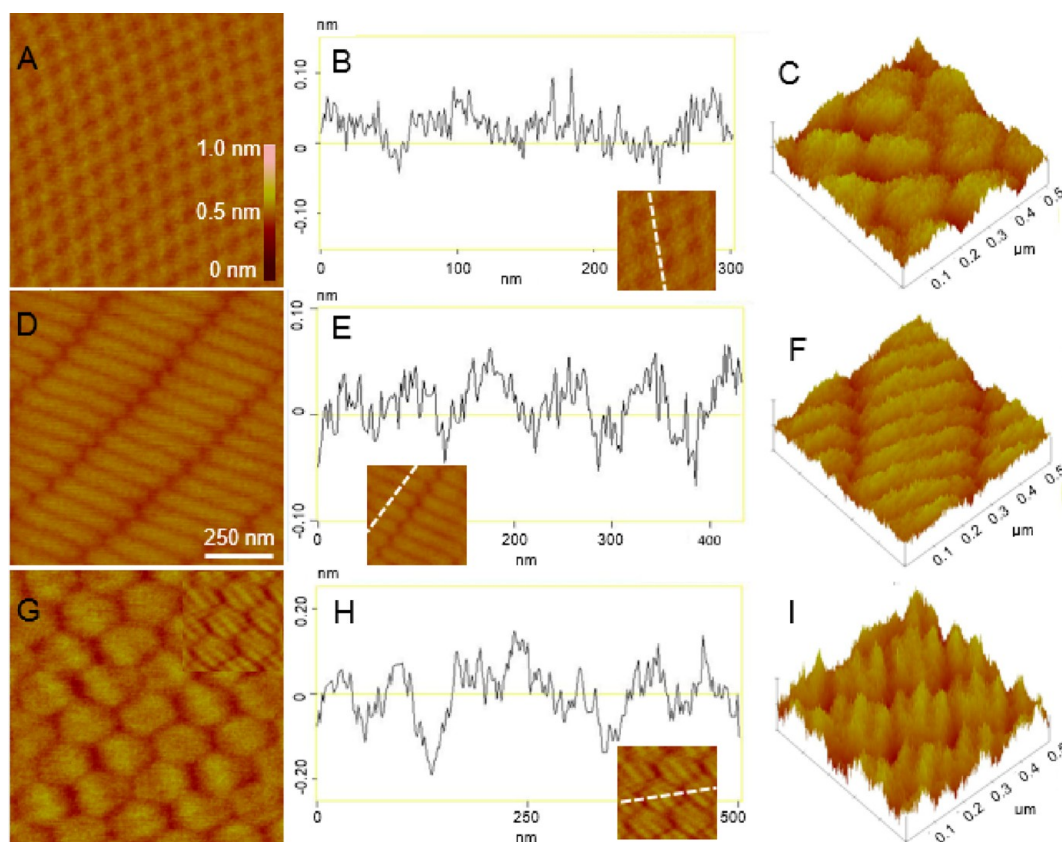
Figure 5. Second group of regular patterns on the muscovite mica surface. Panels A, D, and G are all the height view images obtained by using tapping mode AFM, and they share the same height and length bars. The inset in panel G is its magnified image to show the tri-rod-like units. Panels B, E, and H are the section analysis views for panels A, D, and G, respectively. The white dotted lines in the insets indicate the section cutting lines. Panels C, F, and I are the 3-D views for panels A, D, and G, respectively.

We speculate that this line could be the easily broken-line when peeling off the mica sheet, just like to break the glass by a diamond knife scratching first. The boundaries of the basic unit could also act as broken-lines, which is demonstrated on another two-layered mica surface with the extraordinary patterns shown in Figure 3D,E. The height section analysis of ~0.2 nm for the top-bottom-layer depth indicates the bottom layer is a middle structure layer between the periodic layers of mica crystal structure, which should be formed by peeling off actions due to the unstable atomic bonds inside the boundaries of the basic units. Clearly, though the detailed pattern's shapes are destroyed, the extending orientation of the pattern's alignment can be still distinguished from the middle structured mica layer.

For a closer observation, different morphological patterns are discovered around the defects on the muscovite mica surface. The first group of patterns shown in Figure 4 look like ellipsoids and diamonds. As the basic units of patterns, the dimensions of the diamond (1st row), the mulberry (2nd row), and the ellipsoid (3rd row) are ~369.16 nm (length), ~183.62 nm (long diameter) × ~113.31 nm (short diameter), and ~150.46 nm (long diameter) × 111.38 nm (short diameter), respectively.

In contrast to the first group of patterns above, the second group of patterns show knot-like, rod-like, and tri-parallel-rod-like morphologies from the top to the bottom rows, respectively, in Figure 5. Their dimensions can be described as ~62.209 nm (diameter), ~331.38 nm (length) × ~75.49 nm (width), and ~162.13 nm (length) × ~37.114 nm (width),

respectively. In this group, the basic compromising units are more complicated than those in the first group of patterns, in that all of these three kinds of patterns have an apparent second order of basic units. For instance, both rod (1st ordered) and rod-consisting strip (2nd ordered) could be considered as the basic units of the rod-like patterns in the second row. Moreover, the tri-parallel-rod-like patterns in the third row possess both the rod as the first ordered units and the tri-parallel-rod as the second ordered units. In addition, the knot-net-like patterns are more complicated to describe. It could be better to grasp these patterns by their corresponding visualized 3-D view images beside their section analysis views, which again exhibit the powerful capacity of AFM.

At the first glance from a large scale of the regularly distributed patterns shown from Figure 2 to Figure 5, most probably it may recall some interference/diffraction fringes from the physics point of view. Some literature has reported the large scale hexagonal domain-like structures superimposed on the atomic corrugation of a highly oriented pyrolytic graphite (HOPG) surface by scanning tunnelling microscopy (STM),[31] which was explained by a rotation of the topmost layer relative to its neighboring underlayers of HOPG. Others may call these patterns moiré fringes,[32] which are mostly found on the HOPG surface and observed by STM. To the best of our knowledge, the moiré structures on HOPG are caused by the electronic interference mechanism, and thus can only be observed by STM and not by AFM or transmission electronic microscopy (TEM). By the contact AFM mode in air, Guo et al. created the moiré fringes on the muscovite mica by deliberately tuning the
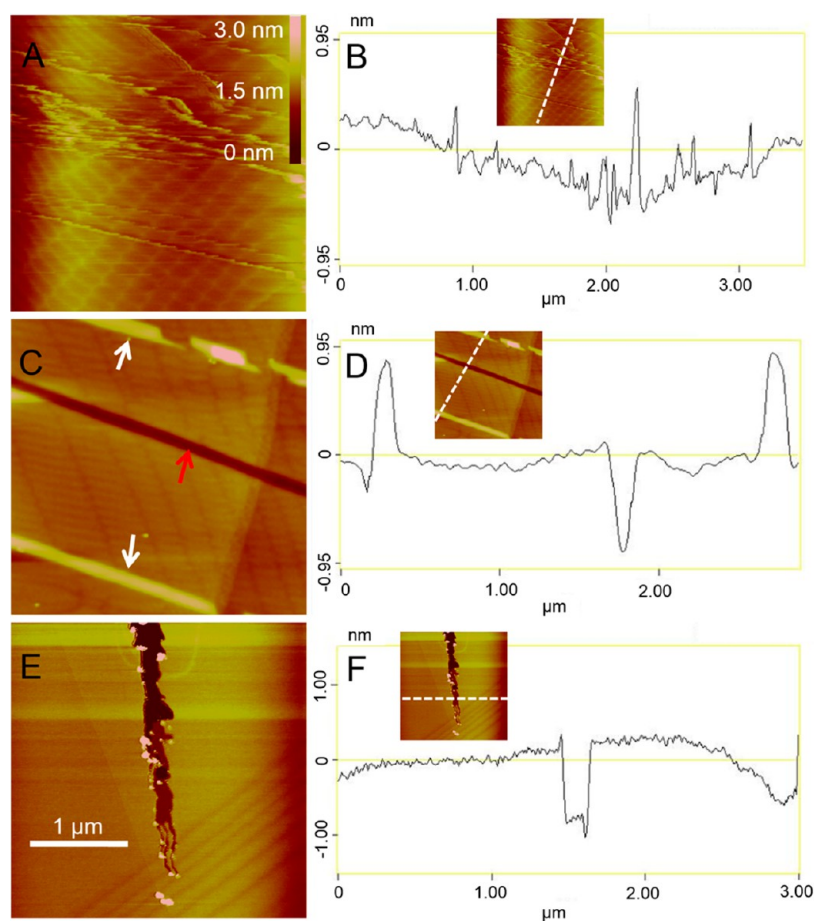
Figure 6. Evidence that the patterns exist real on mica surface. The anomalous patterns coexist with rived structures (A, C) and the man-made scratches (E) on the surface layers of the muscovite mica. Panels A and C were obtained by the contact mode AFM, and panel E was a tapping AFM image. Both the height and length bars applied to all these three height images: panels A, C, and E. In panel C, the groove and rods structures are indicated by red and white arrows, respectively. Panels B, D, and F are the section analysis views for panels A, C, and E, respectively. The white dotted lines in the insets indicate the section cutting lines.

scanning lines to periodically mismatch atomic lattices of the muscovite surface.[32] In other words this kind of moiré fringes are created by the interference between AFM scanning lines and the periodical atomic lattice lines, so they are artificial/man-made visual images and cannot be repeatedly observed by other microscopes which are not based on the line-scanned technique. The similar phenomena was also observed on the HOPG surface by using STM.[32] Because the periodical distance of moiré fringes are normally larger than that of the atomic lattices of crystal surfaces, so the moiré fringes can act as a "magnifier" to examine the matter deformation and surface imperfections of crystal lattices with scanning probe microscopy.[33−35]

Because the tunnelling current results from an overlap of wave functions of the tip with the samples, the STM images essentially represent the properties of the electronic structure of the surfaces, despite the fact that images in some cases closely resemble the geometric surface topography, that is, the atomic arrangement at the surface.[36,37] Some unusual electronic patterns on HOPG were also reported by Choudhary et al., in which they found a particular layer comprises 2-D spatially varying superlattice and 1-D fringes, which was present in a finite region of a layer on the surface confined between two carbon fibers, and the authors attributed this spatially varying superlattice structure to the shear strain generated in the top layer due to the restraining fibers.[38]

As shown in Figure 6A,B, both these images were obtained from the freshly cleaved muscovite mica surface. From Figure 6A, it is clear that the torn edges left on the surface have no influence on the patterns. The section analysis of the neater torn edges in Figure 6B shows that the average height of the two rods (∼0.9 nm) almost equals to the depth of the groove (∼0.9 nm). We postulate that the two rods and the groove structures on this layer surface have the complementary structures as two grooves and one rod on the peeled layer surface. It is also very clear that on the two sides of the groove or rods, the patterns are not continuously orientated but developed independently. Moreover, we have artificially scratched the mica surface by manipulating the AFM tip to examine whether these patterns can be destroyed by some external factors. However, the coexistence of the resulted scratch with a depth of ∼1 nm and the patterns in Figure 6C proved that the patterns found in this report are real, but not similar to those moiré fringes created by scanning based microscopy.

Previously, a disease-related peptide GAV-9 was found to grow epitaxially into nanofilaments on the mica surface in an "upright standing" manner.[12,14,16,39−42] A more interesting experiment, as shown in Figure 7, further in situ proved that the
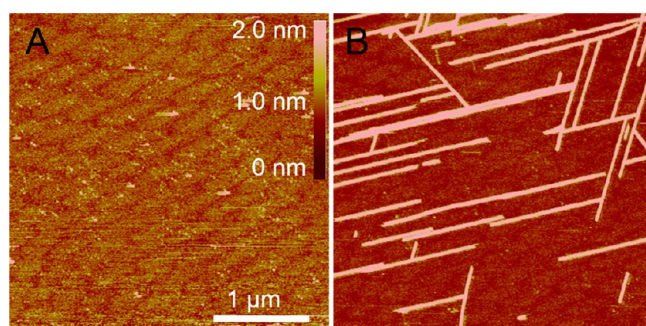
Figure 7. In situ observation of GAV-9 peptide self-assembling on the mica surface with the anomalous patterns. Panel A shows GAV-9 peptides started adsorbing to mica surface after loading the peptide solution onto the mica surface, and panel B shows that the formation of peptide's nanofibrils and the mica's anomalous patterns did not influence each other. Both the height view AFM images were obtained by using the tapping mode AFM in liquid, and they shared the same height and length bars.

external factors such as the peptide self-assembly events cannot influence any to these intrinsic patterns; vice versa, these extraordinary patterns do not influence the template-assisted self-assembly or epitaxial growth of the peptide (GAV-9), either. Moreover, these patterns are independent of the AFM imaging modes (such as contact mode for Figure 4G and Figure 6A,C and tapping mode for all other figures) and the scanning rates/sizes, which overall concludes that they are real but not some AFM artifacts caused by mechanical vibrations, electrical interference, acoustic noise or optical interference.[43]

Muscovite mica is monoclinic with a tendency toward pseudohexagonal crystals. By analyzing the alignment of the basic units from the most regular patterned images (Figure 8), these localized patterns could be shown to somehow mimic 2-D crystals. Moreover, from their cell parameters, all of three patterns are similar to the orthorhombic system, which is a least
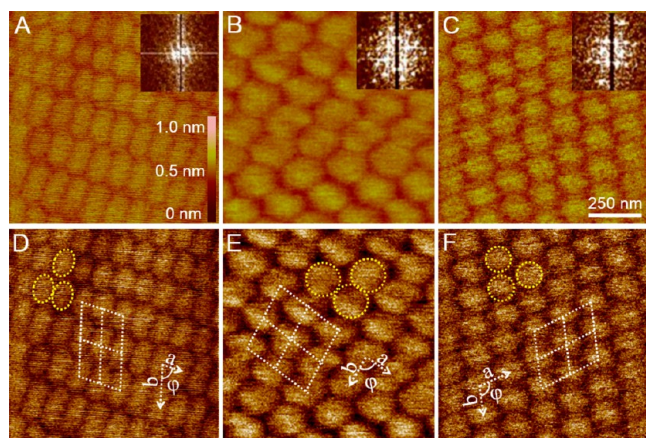

Figure 8. Regular patterns mimic 2-D crystals. The AFM height view images with different regular morphologies (A, B, C) show their periodic spatial distribution (the insets) with the 2-D Fourier transfer function, and the corresponding results are shown in panels D, E and F, respectively. The yellow circles show the minimum units of the 2-D crystal-like patterns. The white rhomboids depict their crystal unit-cells, whose cell parameters are measured as $a = 111.35$ nm, $b = 179.79$, $\varphi = 74.2°$ for panel D, $a = 181.09$ nm, $b = 169.28$, $\varphi = 83.6°$ for panel E and $a = 141.82$ nm, $b = 118$, $\varphi = 107.1°$ for panel F, respectively. Both the height and length bars apply to all the images.

symmetric crystal catalogue with the characteristic cell parameters of $a \neq b$, $\varphi \neq 90°$. Because AFM is unable to detect the nether layers, and the current X-ray crystallography is also difficult to analyze so small of regions, which are rarely localized around the mica defects, so it is hard to identify the 3-D atomic structure of these patterned regions. However, the amazing consistence of the structural characteristics between the most neighboring/adjacent layers revealed by AFM, as shown in Figure 3, can convince us that the current 2-D crystal-like patterns can be extended to 3-D orthorhombic systems, and the third cell parameter c is ~2 nm. This again demonstrates the powerful capacity of AFM in this specific research. Because the formation of mica minerals is a procedure of crystallization under a natural/uncontrolled condition, such defects formation could be inevitable events. Nevertheless, to answer the question how this happens and whether this can be controlled might remain interesting but unknown by the current knowledge of crystallography.

CONCLUSIONS

In conclusion, different natural patterns around the defects on the muscovite mica surface have been discovered and thoroughly analyzed by using AFM. Although we could not explain their formation or even tell the significance of their existence, at least we are able to discover these extraordinary patterns on ever considered mica superflat substrates. Second, we have also proved that these patterns are real but not similar to those moiré fringes formed by either electronic interference on HOPG or by artificial interference between atomic lattice and scanning lines on the mica surface. Third, such patterns have no effect on the template-assisted self-assembly or the epitaxial growth of biomolecules (peptides), which in a certain sense indicates the biomolecule's epitaxial growth, thus allowing some extent of perturbations like the anomalous patterns on the substrates proved in this paper. We hope these extraordinary patterns can draw attention from those who are working with mica as the best super flat substrate for research or industry applications.

AUTHOR INFORMATION

Corresponding Author

*F. Zhang. E-mail: Fengzhang1978@hotmail.com.

Author Contributions

All authors have given approval to the final version of the paper.

Notes

The authors declare no competing financial interest.

■ REFERENCES

(1) Kim, D. T.; Blanch, H. W.; Radke, C. J. Direct Imaging of Lysozyme Adsorption onto Mica by Atomic Force Microscopy. *Langmuir* **2002**, *18*, 5841−5850.

(2) Terashima, H.; Tsuji, T. Adsorption of Bovine Serum Albumin onto Mica Surfaces Studied by a Direct Weighing Technique. *Colloids Surf., B* **2003**, *27*, 115−122.

(3) Hsueh, C.; Chen, H.; Gimzewski, J. K.; Reed, J.; Abdel-Fattah, T. M. Localized Nanoscopic Surface Measurements of Nickel-Modified Mica for Single Molecule DNA Sequence Sampling. *ACS Appl. Mater. Interfaces* **2010**, *2*, 3249−3256.

(4) Czajkowsky, D. M.; Li, L.; Sun, J.; Hu, J.; Shao, Z. Heteroepitaxial Streptavidin Nanocrystals Reveal Critical Role of Proton "Fingers" and Subsurface Atoms in Determining Adsorbed Protein Orientation. *ACS Nano* **2012**, *6*, 190−198.

(5) Falini, G.; Fermani, S.; Conforti, G.; Ripamonti, A. Protein Crystallisation on Chemically Modified Mica Surfaces. *Acta Crystallogr., Sect. D: Biol. Crystallogr.* **2002**, *58*, 1649−1652.

(6) Butt, H. J.; Downing, K. H.; Hansma, P. K. Imaging the Membrane Protein Bacteriorhodopsin with the Atomic Force Microscope. *Biophys. J.* **1990**, *58*, 1473−1480.

(7) Ohnishi, S.; Murata, M.; Hato, M. Correlation between Surface Morphology and Surface Forces of Protein a Adsorbed on Mica. *Biophys. J.* **1998**, *74*, 455−465.

(8) Lau, Y. K. A.; Chernak, D. J.; Bierman, M. J.; Jin, S. Epitaxial Growth of Hierarchical Pbs Nanowires. *J. Mater. Chem.* **2009**, *19*, 934−940.

(9) Utama, M. I.; Peng, Z.; Chen, R.; Peng, B.; Xu, X.; Dong, Y.; Wong, L. M.; Wang, S.; Sun, H.; Xiong, Q. Vertically Aligned Cadmium Chalcogenide Nanowire Arrays on Muscovite Mica: A Demonstration of Epitaxial Growth Strategy. *Nano Lett.* **2011**, *11*, 3051−3057.

(10) Utama, M. I. B.; Belarre, F. J.; Magen, C.; Peng, B.; Arbiol, J.; Xiong, Q. Incommensurate van der Waals Epitaxy of Nanowire Arrays: A Case Study with ZnO on Muscovite Mica Substrates. *Nano Lett.* **2012**, *12*, 2146−2152.

(11) Matolínová, I.; Gillet, M.; Gillet, E.; Matolín, V. A Study of Tungsten Oxide Nanowires Self-Organized on Mica Support. *Nanotechnology* **2009**, *20*, 445604.

(12) Zhang, F.; Du, H.-N.; Zhang, Z.-X.; Ji, L.-N.; Li, H.-T.; Tang, L.; Wang, H.-B.; Fan, C.-H.; Xu, H.-J.; Zhang, Y.; Hu, J.; Hu, H.-Y.; He, J.-H. Epitaxial Growth of Peptide Nanofilaments on Inorganic Surfaces: Effects of Interfacial Hydrophobicity/Hydrophilicity. *Angew. Chem., Int. Ed.* **2006**, *45*, 3611−3613.

(13) Sun, L.-H.; Xu, C.-Y.; Yu, F.; Tao, S.-X.; Li, J.; Zhou, H.; Huang, S.; Tang, L.; Hu, J.; He, J.-H. Epitaxial Growth of Trichosanthin Protein Crystals on Mica Surface. *Cryst. Growth Des.* **2010**, *10*, 2766−2769.

(14) Xie, M.; Li, H.; Ye, M.; Zhang, Y.; Hu, J. Peptide Self-Assembly on Mica under Ethanol-Containing Atmospheres: Effects of Ethanol on Epitaxial Growth of Peptide Nanofilaments. *J. Phys. Chem. B* **2012**, *116*, 2927−2933.

(15) Leow, W. W.; Hwang, W. Epitaxially Guided Assembly of Collagen Layers on Mica Surfaces. *Langmuir* **2011**, *27*, 10907−10913.

(16) Li, H.; Zhang, F.; Zhang, Y.; Ye, M.; Zhou, B.; Tang, Y.-Z.; Yang, H.-J.; Xie, M.-Y.; Chen, S.-F.; He, J.-H.; Fang, H.-P.; Hu, J. Peptide Diffusion and Self-Assembly in Ambient Water Nanofilm on Mica Surface. *J. Phys. Chem. B* **2009**, *113*, 8795−8799.

(17) Poppa, H.; Elliot, A. G. The Surface Composition of Mica Substrates. *Surf. Sci.* **1971**, *24*, 149−163.

(18) Hansma, H. G. Possible Origin of Life between Mica Sheets: Does Life Imitate Mica? *J. Biomol. Struct. Dyn.* **2013**, *31*, 888−895.

(19) Hansma, H. G. Possible Origin of Life between Mica Sheets. *J. Theor. Biol.* **2010**, *266*, 175−188.

(20) Mauguin, C. Ètude Du Mica Muscovite Au Moyen Des Rayons X. *C. R. Hebd. Seances Acad. Sci.* **1927**, *185*, 288.

(21) Butt, H.-J.; Kappl, M. *Surface and Interfacial Forces*, 1st ed; WILEY-VCH Verlag GmbH & Co. KGaA: Weinheim, Germany, 2010.

(22) Ostendorf, F.; Schmitz, C.; Hirth, S.; Kuehnle, A.; Kolodziej, J. J.; Reichling, M. How Flat Is an Air-Cleaved Mica Surface? *Nanotechnology* **2008**, *19*, 1−6.

(23) Müller, K.; Chang, C. C. Electric Dipoles on Clean Mica Surfaces. *Surf. Sci.* **1969**, *14*, 39−51.

(24) de Poel, W.; Pintea, S.; Drnec, J.; Carla, F.; Felici, R.; Mulder, P.; Elemans, J. A. A. W.; van Enckevort, W. J. P.; Rowan, A. E.; Vlieg, E. Muscovite Mica: Flatter Than a Pancake. *Surf. Sci.* **2014**, *619*, 19−24.

(25) Landau, E. M.; Levanon, M.; Leiserowitz, L.; Lahav, M.; Sagiv, J. Transfer of Structural Information from Langmuir Monolayers to Three-Dimensional Growing Crystals. *Nature* **1985**, *318*, 353−356.

(26) Xia, Y. N.; Whitesides, G. M. Soft Lithography. *Angew. Chem., Int. Ed.* **1998**, *37*, 550−575.

(27) Aizenberg, J.; Black, A. J.; Whitesides, G. M. Controlling Local Disorder in Self-Assembled Monolayers by Patterning the Topography of Their Metallic Supports. *Nature* **1998**, *394*, 868−871.

(28) Aizenberg, J.; Black, A. J.; Whitesides, G. M. Control of Crystal Nucleation by Patterned Self-Assembled Monolayers. *Nature* **1999**, *398*, 495−498.

(29) Zhou, P.; Zhang, H. Q.; Zhang, Q.; Liu, Z.; Guan, S.; Wang, G.; Zhou, C.; Jia, J.; Lv, X.; Shao, J.; Cui, Y.; Chen, L.; Chen, X. The Nanostructure Formation on Muscovite Mica Surface Induced by Intermediate-Energy Ions. *Nucl. Instrum. Methods Phys. Res., Sect. B* **2013**, *307*, 221−224.

(30) Metya, A.; Ghose, D.; Mollick, S. A.; Majumdar, A. Nanopatterning of Mica Surface under Low Energy Ion Beam Sputtering. *J. Appl. Phys.* **2012**, *111*, 1−7.

(31) Liu, C. Y.; Chang, H.; Bard, A. J. Large Scale Hexagonal Domainlike Structures Superimposed on the Atomic Corrugation of a Graphite Surface Observed by Scanning Tunneling Microscopy. *Langmuir* **1991**, *7*, 1138−1142.

(32) Guo, H. M.; Liu, H. W.; Wang, Y. L.; Xie, H. M.; Dai, F. L.; Gao, H. J. Moire Fringes of HOPG and Mica in Scanning Probe Microscopy. *Acta Phys. Sin.* **2003**, *52*, 2514−2519.

(33) Xie, H. M.; Shang, H. X.; Xue, Q. K.; Jia, J. F.; Dai, F. L. Defects Analysis of Al/Si Artificial Nanocluster with Moire Fringes. *Opt. Laser. Eng.* **2005**, *43*, 1071−1080.

(34) Fukui, N.; Suwa, Y.; Yoshida, H.; Sugai, T.; Heike, S.; Fujimori, M.; Terada, Y.; Hashizume, T.; Shinohara, H. Moire Image Patterns on Double-Walled Carbon Nanotubes Observed by Scanning Tunneling Microscopy. *Phys. Rev. B* **2009**, *79*, 1−5.

(35) Shang, H. X.; Xie, H. M.; Liu, Z. W.; Guo, H. M.; Gao, H. J.; Dai, F. L. Phase Shifting Nano-Moire Method with Scanning Tunneling Microscope. *Opt. Laser. Eng.* **2004**, *41*, 755−765.

(36) Avouris, P. Atom-Resolved Surface Chemistry Using the Scanning Tunneling Microscope. *J. Phys. Chem.* **1990**, *94*, 2246−2256.

(37) Hansma, P. K. Scanning Tunneling Microscopy. *J. Appl. Phys.* **1987**, *61*, R1−R23.

(38) Choudhary, S. K.; Gupta, A. K. Some Unusual Electronic Patterns on Graphite Surface. *Pramana* **2008**, *70*, 339−350.

(39) Zhou, X.; Li, R.; Dai, B.; Zhang, Y.; Xu, P.; Zhang, Y. The Fabrication and Electrical Characterization of Protein Fibril-Templated One-Dimensional Palladium Nanostructures. *Eur. Polym. J.* **2013**, *49*, 1957−1963.

(40) Zhou, X.; Zheng, L.; Li, R.; Li, B.; Pillai, S.; Xu, P.; Zhang, Y. Biotemplated Fabrication of Size Controlled Palladium Nanoparticle Chains. *J. Mater. Chem.* **2012**, *22*, 8862−8867.

(41) Dai, B.; Kang, S.-g.; Tien, H.; Lei, H.; Castelli, M.; Hu, J.; Zhang, Y.; Zhou, R. Salts Drive Controllable Multilayered Upright Assembly of Amyloid-like Peptides at Mica/Water Interface. *Proc. Natl. Acad. Sci. U. S. A.* **2013**, *110*, 8543−8548.

(42) Hou, J.-H.; Du, Q.-Q.-G.; Zhong, R.-B.; Zhang, P.; Zhang, P., Temperature Manipulating Peptide Self-Assembly in Water Nanofilm. *Nucl. Sci. Technol.* **2014**, *25*.

(43) Méndez-Vilas, A.; González-Martín, M. L.; Nuevo, M. J. Optical Interference Artifacts in Contact Atomic Force Microscopy Images. *Ultramicroscopy* **2002**, *92*, 243−250.